Title

Executioner caspase is proximal to Fasciclin 3 which facilitates non-lethal activation in *Drosophila* olfactory receptor neurons

Short title

Fasciclin 3 non-lethally activates caspase in *Drosophila* olfactory neurons

Authors

Masaya Muramoto[a,1], Nozomi Hanawa[a,1], Misako Okumura[b,c], Takahiro Chihara[b,c], Masayuki Miura[a,2], and Natsuki Shinoda[a,2]

Affiliations & Footnotes

[a]Department of Genetics, Graduate School of Pharmaceutical Sciences, University of Tokyo, 7-3-1 Hongo, Bunkyo-ku, Tokyo 113-0033, Japan

[b]Department of Biological Science, Graduate School of Science, Hiroshima University, Higashi-Hiroshima, Hiroshima 739-8526, Japan

[c]Program of Biomedical Science and Basic Biology, Graduate School of Integrated Sciences for Life, Hiroshima University, Higashi-Hiroshima, Hiroshima 739-8526, Japan

[1]Equal contributions

[2]Corresponding authors

Corresponding Authors

Masayuki Miura: Department of Genetics, Graduate School of Pharmaceutical Sciences, University of Tokyo, 7-3-1 Hongo, Bunkyo-ku, Tokyo 113-0033, Japan. Telephone: +81-3-5841-4860. E-mail: miura@mol.f.u-tokyo.ac.jp

Natsuki Shinoda: Department of Genetics, Graduate School of Pharmaceutical Sciences, University of Tokyo 7-3-1 Hongo, Bunkyo-ku, Tokyo 113-0033, Japan. Telephone: +81-3-5841-4867. E-mail: f-shinoda.natsuki@g.ecc.u-tokyo.ac.jp

Author Contributions

Masaya Muramoto: Formal Analysis, Investigation, Methodology, Resources, Writing – Review & Editing; Nozomi Hanawa: Formal analysis, Investigation, Methodology, Resources, Writing – Review & Editing; Misako Okumura: Methodology, Writing – Review & Editing; Takahiro Chihara: Methodology, Writing – Review & Editing; Masayuki Miura: Conceptualization, Funding Acquisition, Supervision, Writing – Original Draft Preparation; Natsuki Shinoda: Conceptualization, Formal Analysis, Funding Acquisition, Investigation, Project Administration, Supervision, Validation, Visualization, Writing – Original Draft Preparation

Conflict of Interest

The authors declare that they have no conflict of interest.

Abstract

Executioner caspases are activated by initiator caspases, resulting in lethal and non-lethal cellular outcomes. Despite the identification of numerous caspase-dependent non-lethal cellular processes (CDPs), the molecular mechanism that enables precise regulation of the non-lethal functions of executioner caspases remains unclear. Here, we conducted a comprehensive analysis of endogenous proximal proteins of *Drosophila* executioner caspases *in vivo* using TurboID. We discovered that in the adult brain, the executioner caspase Drice is primarily proximal to membrane proteins, including the cell adhesion molecule Fasciclin 3 (Fas3). Notably, Drice is proximal to the specific alternative splicing isoforms of Fas3G. To investigate whether Fas3 modulates caspase activity, we developed a Gal4-Manipulated Area-Specific CaspaseTracker/CasExpress (MASCaT) system for highly sensitive monitoring of non-lethal caspase activity near membrane compartments. Using MASCaT, we demonstrated that Fas3 promoted caspase activation near membrane compartments in olfactory receptor neurons without killing them. Activation regulates innate olfactory attraction behavior. Collectively, our findings suggest that the proximal proteins of executioner caspases provide a compartmentalized platform for non-lethal caspase activation and function.

Author Summary

Caspases are Cysteine-ASPartic acid proteASEs which are primarily involved in cell death. In addition, caspases play versatile non-lethal (non-cell death) roles in a wide range of cell types including neurons. However, the molecular mechanism that enables the precise regulation of non-lethal activation and functions remains unclear. Here, we focused on the proximal proteins of caspases as potential regulators of non-lethal activation. By comprehensively analyzing the proximal proteins of caspases in the adult *Drosophila* brain using TurboID, we discovered that caspases are primarily proximal to membrane proteins rather than to cytosolic proteins. By developing a genetic tool that enables highly sensitive monitoring of non-lethal caspase activity near membrane compartments, we found that proximal proteins facilitate non-lethal caspase activation in olfactory receptor neurons. Importantly, non-lethal caspase activation in olfactory receptor neurons affects organismal innate attraction behavior. Our research suggests that a compartmentalized platform established by proximal proteins enables precise regulation of non-lethal caspase activation and function.

72 **Introduction**

73 Caspases are cysteine aspartic acid proteases involved in cell death. Apoptotic stimuli activate
74 initiator caspases that trigger a proteolytic cascade, leading to the activation of executioner
75 caspases and culminating in apoptosis (Fig. 1A) [1]. Caspases exhibit diverse non-lethal cellular
76 functions [2]. In the nervous system, non-lethal caspase activity promotes the maturation of
77 olfactory sensory neurons during development [3]. Furthermore, non-lethal caspase activity
78 induces long-term depression through AKT cleavage [4]. These are termed caspase-dependent
79 non-lethal cellular processes (CDPs) [5]. Despite the discovery of numerous CDPs over the past
80 two decades, the molecular mechanism that underlies specific non-lethal functions without
81 causing cell death remains unclear.

82 Proteins that interact with initiator caspases are among the key regulators of CDPs.
83 Tango7, the *Drosophila* translation initiation factor eIF3 subunit m, acts as an adapter and
84 regulates the localization of the initiator caspase Dronc. During sperm individualization,
85 Tango7 directs Dronc to the individualization complex [6]. In salivary glands, Tango7 directs
86 Dronc to the plasma membrane [7]. In both cases, caspase activity promotes cellular remodeling
87 without inducing cell death [6,7]. CRINKLED, a *Drosophila* unconventional myosin, functions
88 as an adaptor of Dronc and facilitates the cleavage of Shaggy46 [8]. Shaggy46, activated by
89 caspase-mediated cleavage, suppresses the emergence of ectopic sensory organ precursors [9].
90 During apoptosis-induced proliferation (AiP), Myo1D, another *Drosophila* unconventional
91 myosin, facilitates Dronc translocation to the basal side of the plasma membrane of imaginal
92 discs to promote AiP [10]. Thus, initiator caspase-interacting proteins regulate caspase activity
93 in CDPs. However, given the importance of executioner caspases, which cleave a broad range
94 of substrates and are essential for apoptosis [11,12], little is known about the subcellular
95 compartmentalization and interacting proteins of those involved in CDPs. This lack of

96 understanding is partly due to the absence of protein-protein interaction domains (e.g., DED
97 and CARD) in the N-terminus of executioner caspases [13].

98 To understand the molecular mechanism of function of caspases involved in CDPs, we
99 focused on the proximal proteins of executioner caspases using TurboID, a proximity labeling
100 technique that analyzes protein proximity *in vivo* [14,15]. We previously established C-terminal
101 TurboID knocked-in caspase fly lines for Dronc, Drice, and Dcp-1 [16]. Importantly, we have
102 demonstrated that one of the preferred substrates of Drice, BubR1, is proximal to Drice *in vivo*
103 [17], suggesting that substrate preference is exploited by protein proximity. Therefore, the
104 proximity of executioner caspases to proteins is emerging as a means of regulating specific non-
105 lethal functions.

106 In this study, through a comprehensive analysis of proximal proteins, we discovered
107 that the cell adhesion molecule Fasciclin 3 (Fas3) is in close proximity to the executioner
108 caspase Drice in the adult brain. We observed that Drice was exclusively proximal to specific
109 alternative splicing isoforms of Fas3. To ascertain whether Fas3 modulates caspase activity, we
110 developed a Gal4-Manipulated Area Specific CaspaseTracker/CasExpress (MASCaT) system,
111 which permits the monitoring of caspase activity with high sensitivity and simultaneous genetic
112 manipulation in the cells of interest. Using MASCaT, we demonstrated that Fas3 enhances
113 caspase activation without killing cells. Subsequently, we showed that activation regulates
114 innate olfactory attraction behavior. Collectively, our findings suggest that the proximal
115 proteins of executioner caspases provide a compartmentalization platform that enables the
116 precise regulation of non-lethal caspase activation and function.

117 **Results**

118 ***Drice is the major executioner caspase expressed in the adult brains***

119 In *Drosophila*, the caspase-mediated apoptotic signaling pathway is highly conserved [2]. The
120 activity of executioner caspases, specifically Drice and Dcp-1, is regulated by apoptotic
121 signaling pathways, including the initiator caspase Dronc (Fig. 1A). To investigate the
122 expression patterns of *Drosophila* caspases, we employed *Caspase::V5::TurboID* knocked-in
123 fly lines [16]. We found low levels of expression of the initiator caspase Dronc in adult heads
124 (Fig. 1B). Conversely, we observed high expression of the executioner caspase Drice, whereas
125 Dcp-1 was expressed at lower levels in adult heads (Fig. 1B). The proximal proteins of each
126 caspase were labeled with TurboID in adult heads by administration of 100 μM biotin (Fig. 1B).
127 Furthermore, we investigated the expression patterns of caspases using histochemical analysis
128 by examining streptavidin (SA) signal. Consistent with the western blotting findings, Drice
129 showed higher expression levels than Dronc and Dcp-1, which were expressed at lower levels
130 (Fig. 1C). We found that Drice was expressed in distinct regions, including the mushroom
131 bodies (MBs), suboesophageal ganglions (SGs), optic lobes (OLs), and antennal lobes (ALs),
132 which showed the highest levels of expression (Fig. 1C). The *Drosophila* AL comprise synaptic
133 contacts between the axons of olfactory receptor neurons (ORNs), the dendrites of projection
134 neurons (PNs), and local interneuron (LNs) processes. Neuron-type-specific Gal4s were used
135 to knockdown *Drice* and the expression patterns were subsequently examined. We found that
136 Drice was expressed predominantly in ORNs in the AL (Fig. 1D). These results suggest that
137 Drice is the major executioner caspase that regulates both lethal and non-lethal functions of
138 adult ORNs.

139

140 ***Drice is proximal to membrane proteins rather than cytosolic proteins in the adult brains***

141 To comprehensively identify proximal proteins of Drice, we employed a proximity labeling
142 approach. Specifically, we used *Drice::V5::TurboID* flies fed 100 μM biotin. We confirmed
143 biotinylation of Drice proximal proteins in the adult brain (Fig. 1E). After purifying the
144 biotinylated proteins using NeutrAvidin magnetic beads, we performed LC-MS/MS analysis of
145 the samples (Fig. 1F). We identified 643 proteins (Fig. 1G, Table S1), of which 158 were highly
146 specific to *Drice::V5::TurboID* flies compared to wild-type flies (*Drice::V5::TurboID*/w^{1118} >
147 10; Fig. 1G, Table S1). Gene ontology analysis revealed that Drice proximal proteins were
148 enriched in the plasma membrane, synaptic vesicles, postsynaptic membranes, and adherens
149 junctions (Fig. 1H, Table S2). This finding suggests that Drice is localized primarily in
150 membrane compartments rather than in the cytoplasm of the adult brain. Additionally, because
151 the SA signal of *Drice::V5::TurboID* is mainly observed in the AL where the axons of ORNs
152 project (Fig. 1C), the enrichment of membrane proteins in the proximal proteins of Drice is
153 reasonable.
154
155 ***A specific splicing isoform of Fasciclin 3 is in proximity to Drice***
156 Among the identified neighboring proteins of Drice, we focused on Fasciclin 3 (Fas3) [18], a
157 transmembrane protein containing immunoglobulin-like domains that regulates synaptic target
158 recognition and axon fasciculation [19]. The role of Fas3 in apoptosis remains unclear. The
159 expression patterns of Fas3 in the adult brain were similar to those of Drice, particularly in the
160 OLs, SGs, and ALs (Fig. 2A, B). Fas3 is encoded by seven splicing isoforms, resulting in the
161 production of five protein isoforms that share extracellular domains but differ in intracellular
162 domains with low-complexity sequences (Fig. 2C-E). Only one specific protein isoform, Fas3
163 isoform G (Fas3G), was identified in the LC-MS/MS analysis as a Drice proximal protein in
164 the adult brain (Fig. 1G, Table S1). To validate this result, we generated an antibody specific
165 to Fas3G (Fig. 2D, F). We confirmed that only the Fas3G was labeled with *Drice::V5::TurboID*

166 and purified using NeutrAvidin magnetic beads as detected using western blotting (Fig. 2G).
167 To further confirm the isoform specificity to Drice proximity, we overexpressed 3xFLAG-
168 tagged Fas3 isoforms A, B/F, C, D/E, and G in olfactory receptor neurons using *Pebbled-Gal4*
169 in a *Drice::V5::TurboID* background. After proximity labeling with TurboID, followed by
170 NeutrAvidin purification, we found that the Fas3G was highly enriched compared to the other
171 isoforms (Fig. 2H). These findings suggested that Drice is proximal to a specific isoform of
172 Fas3 in olfactory receptor neurons, regardless of its protein expression level.
173
174 ***MASCaT: a cell type-specific highly sensitive non-lethal caspase activity reporter***
175 We investigated whether Fas3 regulates caspase activity in lethal or non-lethal processes.
176 CaspaseTracker/CasExpress is a highly sensitive reporter of non-lethal caspase activity that
177 uses caspase-activatable Gal4 tethered to the membrane by mCD8 [20,21]. However, reliance
178 on Gal4 to report their activity presents a challenge in reconciling Gal4/UAS-dependent gene
179 manipulations. To overcome this limitation, we developed a novel reporter that captures non-
180 lethal caspase activation independently of the Gal4/UAS system. Specifically, we replaced
181 caspase-activatable Gal4 with caspase-activatable QF2 (mCD8::DQVD::QF2), where DQVD
182 is a caspase cleavage site, and generated *Ubi-FRT-STOP-FRT-mCD8::DQVD::QF2*,
183 simultaneously expressing *Flippase* (*FLP*) under *UAS* to restrict reporter expression to the cells
184 of interest (Fig. 3A). As a negative control, we created caspase-non-activatable QF2
185 (mCD8::DQVA::QF2). *Drosophila* S2 cells undergo weak caspase activation only by
186 transfection [17]. Taking advantage of that, this system reports caspase activity through the
187 caspase-activatable QF2/QUAS system, expressing mNeonGreen, which is not detected by
188 caspase-non-activatable QF2 (Fig. 3B). We named this novel reporter a Gal4-Manipulated Area
189 Specific CaspaseTracker/CasExpress (MASCaT; Fig. 3A). Utilizing MASCaT, we detected
190 non-lethal caspase activity, specifically in the neurons of adult brains, using *ELAV-Gal4* (Fig.

191 3C). Caspase activity was prominent in OLs (Fig. 3C), which is consistent with the previously
192 reported activation pattern of caspase detected by CaspaseTracker/CasExpress [20,21].
193 Previously, we reported that a specific subset of ORNs, including Or42b, undergoes age-
194 associated caspase activation [22]. Consistent with this finding, we detected age-dependent
195 caspase activation in the AL (Fig. 3C). Therefore, our newly established reporter, MASCaT,
196 enables the highly sensitive detection of caspase activity near the membrane in cells of interest
197 in a Gal4/UAS-dependent manner.
198
199 ***Fas3G activates caspase in a non-lethal manner that regulates innate attraction behavior***
200 To investigate the regulatory role of Fas3 in caspase activity *in vivo*, we used Or42b neurons as
201 a model, which have previously been shown to undergo age-dependent caspase activation [22].
202 Initially, we evaluated the effects of Dronc overexpression on apoptosis by quantifying cell
203 body numbers in the antenna in young flies. Dronc induced cell loss while catalytically inactive
204 Dronc ($Dronc^{CG}$) did not, suggesting that Dronc induce apoptosis in a catalytic-dependent
205 manner (Fig. 4A, B). We then evaluated the effects of the overexpression of the executioner
206 caspases Dcp-1 and Drice. Interestingly, although Dcp-1 induced complete cell loss, Drice did
207 not (Fig. 4A, B). These results indicate that Drice requires an initiator caspase for activation,
208 whereas Dcp-1 does not (Fig. 4A, B). Furthermore, the expression of Fas3G, even in
209 combination with Drice, did not reduce the number of cells, implying that Fas3G did not induce
210 apoptosis (Fig. 4C, D).
211 Subsequently, we assessed the regulation of non-lethal caspase activity by Fas3G *in*
212 *vivo*. We first confirmed that MASCaT probes were distributed in the axons of olfactory
213 receptor neurons (Fig. 4E). Using MASCaT, we observed weak non-lethal caspase activation
214 even in the control group at a young age (Fig. 4F, G). The expression of *Fas3G* significantly
215 promoted caspase activation (Fig. 4F, G), indicating that Fas3G regulates non-lethal caspase

216 activation. Moreover, the simultaneous expression of Drice and Fas3G significantly enhanced
217 caspase activation, signifying the promoting effect of their proximity (Fig. 4F, G). Additionally,
218 knockdown or expression of the dominant-negative form of Dronc suppressed Fas3G-
219 facilitated non-lethal caspase activation (Fig. 4H, I), suggesting that this activation is initiator
220 caspase-dependent. Thus, our findings indicate that the proximal proteins of executioner
221 caspases facilitate non-lethal caspase activation in close proximity to the membrane (Fig. 4J).
222 Finally, we examined the function of by Fas3G-facilitated non-lethal caspase activation.
223 Apple cider vinegar (ACV) excites six glomeruli, including DM1, which are innervated by the
224 axons of Or42b neurons [23]. We have previously reported that Or42b neurons undergo aging-
225 dependent caspase activation, which reduces neural activity and attraction behavior in response
226 to ACV [22]. Inhibition of caspase activity in aged flies restores attraction behavior but does
227 not affect that of young flies [22]. Using a two-choice preference assay with ACV, we found
228 that the expression of Fas3G, which activates caspases, did not impair attraction behavior in
229 young flies (Fig. 4K, L). In contrast, simultaneous inhibition of Fas3G-facilitated non-lethal
230 caspase activation promoted attraction to ACV (Fig. 4K, L). Overall, these results suggest that
231 Fas3G-facilitated non-lethal caspase activation suppresses innate attractive behavior without
232 killing the cells.

233 **Discussion**

234 ***Proximal proteins of executioner caspases regulate non-lethal caspase activity***

235 It is important to identify the proximal proteins of executioner caspases, which cleave a wide
236 range of substrates and are essential for apoptosis [11,12], as proximity often dictates substrate
237 specificity [17]. In humans, Caspase-3 and Caspase-7 have been shown to share but also have
238 discrete substrate preferences [24]. Caspase-7 leverages an exosite to facilitate interaction with
239 RNA and enhance the proteolysis of RNA-binding proteins [25,26]. Thus, protein proximity
240 can be used to precisely regulate specific cellular functions by selectively cleaving a limited
241 pool of substrates in non-lethal scenarios. Our current investigation showed that executioner
242 caspases are exclusively sequestered in specific subcellular domains, including the plasma
243 membrane. We identified Fas3G as a regulator of non-lethal activation, underscoring the
244 importance of protein proximity not only in substrate cleavage, but also in localizing non-lethal
245 activation to the vicinity of plasma membrane (Fig. 4J).

246

247 ***MASCaT as a highly sensitive reporter for identifying non-lethal caspase regulators***

248 Various caspase activity reporters have been developed, including SCAT3, a FRET-based
249 reporter with superior temporal resolution [27], CaspaseTracker/CasExpress, Caspase-
250 activatable Gal4-based reporters with superior sensitivity [20,21]. However, to date, no reporter
251 has been developed that is sensitive enough to identify non-lethal regulators of caspases in cells
252 of interest. In this study, we developed a novel caspase reporter, MASCaT, that can detect non-
253 lethal caspase activation with high sensitivity in a cell type-specific manner following gene
254 manipulation. Using MASCaT, we identified previously overlooked regulators of non-lethal
255 activation of caspases in a cell type-specific manner. Proximal proteins of executioner caspases
256 are potential non-lethal regulators, and combining TurboID-mediated identification of these

257 proteins will pave the way for identifying non-lethal components and broaden our
258 understanding of the molecular mechanism of non-lethal caspase activation.
259
260 ***Non-lethal caspase activation regulates neural activity and behaviors***
261 We previously reported that age-dependent caspase activation reduces neural activity and innate
262 attraction behavior [22]. Here, we found that, while Fas3G expression did not impair attraction
263 behavior by itself, caspase activation upon Fas3G overexpression suppressed attraction
264 behavior toward ACV (Fig. 4K, L). In mice, L1CAM, an immunoglobulin-like cell adhesion
265 molecule, facilitates neuronal excitability by regulating the voltage-gated Na+ channels [28].
266 Thus, we hypothesize that non-lethal caspase activation antagonizes the neuronal excitability
267 promoted by Fas3G. In neurons, caspases have diverse non-lethal functions, including axon
268 degeneration and macro- and micro-pruning, to regulate synaptic plasticity [29,30]. In
269 presynaptic terminals, it has been recently reported that Caspase-3 modulates synaptic vesicle
270 pools via autophagy [31]. Thus, it is possible that non-lethal activation regulates synaptic pools
271 and neural activity in a reversible manner without killing the cells. Analyzing the functions
272 mediated by Drice/Fas3G proximity, including the identification of specific substrates, will
273 pave the way for identifying diverse CDPs and understanding their molecular mechanisms.
274 While suppressing innate attraction behavior does not seem beneficial by itself, it should
275 be a great advantage in decision-making. To survive, flies must constantly make appropriate
276 behavioral decisions (e.g., feeding versus mating) depending on their physiological conditions.
277 In males, a subset of neurons regulated by tyramine controls feeding versus mating behaviors
278 [32]. In regard of that, it is important to adequately promote/suppress neural activity, which
279 controls behaviors of the organisms, by precisely controlling caspase activation in a
280 compartmentalization-dependent manner in neurons.
281

282 ***How does Fasciclin 3 regulate non-lethal caspase activation?***

283 Although the core apoptotic machinery has been well characterized during the last 30 years [2],
284 the precise regulation of CDPs, remains incompletely elucidated. In this study, we identified
285 Fas3 as a context-specific activator of Drice. However, the mechanism by which Fas3G
286 regulates non-lethal activation is still an unresolved question in our research. Notably, Fas3G
287 was not a determinant of apoptosis, since overexpression of Fas3G did not reduce the number
288 of ORNs (Fig. 4C, D). Fas3 is an immunoglobulin-like domain-containing transmembrane
289 protein that regulates axonal fasciculation and neuronal projections [18]. NCAM, a mammalian
290 homologue of Fascicilin 2, is an immunoglobulin-like domain-containing cell adhesion
291 molecule. NCAM can physically bind to Caspase-8, and depending on NCAM clustering,
292 Caspase-8 and -3 are activated and contribute to neurite outgrowth by cleaving its substrate
293 spectrin [33]. Thus, it is possible that Fas3G physically binds to the initiator caspase Dronc,
294 which is required for Fas3G-facilitated non-lethal caspase, to activate Drice.

295 Recently, a protein interactome analysis in humans showed that tissue-preferentially
296 expressed proteins that interact with known apoptosis regulators participate in apoptosis
297 sensitization [34]. Given that CDPs are often cell-and tissue type-specific processes, the
298 identification of modulators of context-dependent apoptotic pathways will aid in understanding
299 the precise molecular regulation of CDPs. Importantly, alternative splicing can diversify
300 protein-protein interaction networks. A recent report showed that minor spliceosomes regulate
301 alternative splicing, including Fas3. A specific isoform of Fas3 has distinct functions and cannot
302 be substituted by other isoforms during neuronal development [35]. Our results support the idea
303 that alternative splicing may not only diversify the protein itself, but also its interaction
304 networks to regulate module-dependent activation. Further interactome analysis using TurboID
305 will reveal the regulatory mechanisms of the non-lethal activation of caspases.

306 **Materials and Methods**

307 ***Fly strains and rearing conditions***

308 We raised the flies in standard *Drosophila* medium at 25°C. For in vivo biotin labeling
309 experiments, flies were raised in standard *Drosophila* medium supplemented with 100 μM (+)-
310 biotin (#132-02635, WAKO). The following fly strains were used in this study: w^{1118},
311 *Drice::V5::TurboID*, *Dcp-1::V5::TurboID*, *Dronc::V5::TurboID* [16], *Pebbled-Gal4*
312 (BL80570), *LN-Gal4* (BL63325), *GH146-Gal4* (BL30026), *UAS-Drice-RNAi* (V28065),
313 *Fas3::EGFP::FlAsH::StrepII::TEV::3xFLAG* (BL59809), *UASz-Fas3A::3xFLAG*, *UASz-*
314 *Fas3B::3xFLAG*, *UASz-Fas3C::3xFLAG*, *UASz-Fas3D::3xFLAG*, *UASz-Fas3G::3xFLAG*
315 (this study), *Ubi-FRT-STOP-FRT-mCD8::DQVD::QF2*, *Ubi-FRT-STOP-FRT-*
316 *mCD8::DQVA::QF2* (this study), *UAS-FLP* (K107788), *QUAS-tdTomato::3xHA* (BL30005),
317 *ELAV-Gal4* (BL8765), *Or42b-Gal4* (BL9971), *UAS-RedStinger* (BL8547), *UASz-*
318 *myc::mNeonGreen*, *UASz-Drice::myc::mNeonGreen* (this study), *UASz-V5::TurboID*, *UASz-*
319 *Drice::V5::TurboID*, *UASz-Drice*^{CG}*::V5::TurboID*, *UASz-Dcp-1::V5::TurboID*, *UASz-Dcp-*
320 *1*^{CG}*::V5::TurboID*, *UASz-Dronc::V5::TurboID*, *UASz-Dronc*^{CG}*::V5::TurboID* (this study),
321 *UAS-Dronc-RNAi* [9], *UAS-Dronc*^{DN} (a gift from H. Richardson). BL, Bloomington Drosophila
322 Resource Center; K, Kyoto Stock Center; V, Vienna Drosophila Resource Center.

323

324 ***Detailed genotypes***

325 Fig. 1B, C (Left to Right, Top to Bottom)

326 w^{1118}*/Y*

327 *w/Y; Dcp-1::V5::TurboID/+*

328 *w/Y;; Drice::V5::TurboID/+*

329 *w/Y;; Dronc::V5::TurboID/+*

330

331 Fig. 1D (Left to Right)

332 *w; UAS-Drice-RNAi/+; Drice::V5::TurboID/+*

333 *w, Pebbled-Gal4/w; UAS-Drice-RNAi/+; Drice::V5::TurboID/+*

334 *w; UAS-Drice-RNAi/GH146-Gal4; Drice::V5::TurboID/+*

335 *w; UAS-Drice-RNAi/+; Drice::V5::TurboID/LN-Gal4*

336

337 Fig. 1E (Left to Right)

338 w^{1118}/Y

339 *w/Y;; Drice::V5::TurboID/+*

340

341 Fig. 1G (Left to Right)

342 w^{1118}/Y

343 *w/Y;; Drice::V5::TurboID/+*

344

345 Fig. 2A (Left to Right)

346 w^{1118}/Y

347 *w/Y;; Drice::V5::TurboID/+*

348

349 Fig. 2B (Top to Bottom, Left to Right)

350 w^{1118}/Y

351 *w/Y;; Drice::V5::TurboID/+*

352 *w/Y; Fas3::EGFP::FlAsH::StrepII::TEV::3xFLAG/+*

353 *w/Y; Fas3:: EGFP::FlAsH::StrepII::TEV::3xFLAG/+; Drice::V5::TurboID/+*

354

355 Fig. 2F (Left to Right)

356 *w, Pebbled-Gal4/w or Y*

357 *w, Pebbled-Gal4/w or Y;; UASz-Fas3A::3xFLAG/+*

358 *w, Pebbled-Gal4/w or Y;; UASz-Fas3B::3xFLAG/+*

359 *w, Pebbled-Gal4/w or Y;; UASz-Fas3C::3xFLAG/+*

360 *w, Pebbled-Gal4/w or Y;; UASz-Fas3D::3xFLAG/+*

361 *w, Pebbled-Gal4/w or Y;; UASz-Fas3G::3xFLAG/+*

362

363 Fig. 2G (Left to Right)

364 w^{1118}/Y

365 *w/Y;; Drice::V5::TurboID/+*

366

367 Fig. 2H (Left to Right)

368 *w, Pebbled-Gal4/w or Y;; Drice::V5::TurboID/+*

369 *w, Pebbled-Gal4/w or Y;; Drice::V5::TurboID/UASz-Fas3A::3xFLAG*

370 *w, Pebbled-Gal4/w or Y;; Drice::V5::TurboID/UASz-Fas3B::3xFLAG*

371 *w, Pebbled-Gal4/w or Y;; Drice::V5::TurboID/UASz-Fas3C::3xFLAG*

372 *w, Pebbled-Gal4/w or Y;; Drice::V5::TurboID/UASz-Fas3D::3xFLAG*

373 *w, Pebbled-Gal4/w or Y;; Drice::V5::TurboID/UASz-Fas3G::3xFLAG*

374

375 Fig. 3C (Top to Bottom)

376 *w/Y; Ubi-FRT-STOP-FRT-mCD8::DQVD::QF2/+; UAS-FLP, QUAS-tdTomato::3xHA/+*

377 *w/Y; Ubi-FRT-STOP-FRT-mCD8::DQVA::QF2/ELAV-Gal4; UAS-FLP, QUAS-*

378 *tdTomato::3xHA/+*

379 *w/Y; Ubi-FRT-STOP-FRT-mCD8::DQVD::QF2/ELAV-Gal4; UAS-FLP, QUAS-*

380 *tdTomato::3xHA/+*

381

382 Fig. 4A, B (Top to Bottom, Left to Right)

383 *w/Y; Or42b-Gal4/+; UAS-RedStinger/UASz-V5::TurboID*

384 *w/Y; Or42b-Gal4/+; UAS-RedStinger/UASz-Drice^{CG}::V5::TurboID*

385 *w/Y; Or42b-Gal4/+; UAS-RedStinger/UASz-Drice::V5::TurboID*

386 *w/Y; Or42b-Gal4/+; UAS-RedStinger/UASz-Dcp-1^{CG}::V5::TurboID*

387 *w/Y; Or42b-Gal4/+; UAS-RedStinger/UASz-Dcp-1::V5::TurboID*

388 *w/Y; Or42b-Gal4/+; UAS-RedStinger/UASz-Dronc^{CG}::V5::TurboID*

389 *w/Y; Or42b-Gal4/+; UAS-RedStinger/UASz-Dronc::V5::TurboID*

390

391 Fig. 4C, D (Top to Bottom, Left to Right)

392 *w/Y; Or42b-Gal4/UASz-3xFLAG::mNeonGreen; UAS-RedStinger/+*

393 *w/Y; Or42b-Gal4/+; UAS-RedStinger/UASz-Fas3G::3xFLAG*

394 *w/Y; Or42b-Gal4/UASz-Drice::myc::mNeonGreen; UAS-RedStinger/+*

395 *w/Y; Or42b-Gal4/UASz-Drice::myc::mNeonGreen; UAS-RedStinger/UASz-Fas3G::3xFLAG*

396

397 Fig. 4E (Top to Bottom)

398 *w/Y; Or42b-Gal4/UASz-3xFLAG::mNeonGreen*

399 *w/Y; Or42b-Gal4, Ubi-FRT-STOP-FRT-mCD8::DQVD::QF2/UASz-3xFLAG::mNeonGreen;*

400 *UAS-FLP, QUAS-tdTomato::3xHA/+*

401

402 Fig. 4F, G (Top to Bottom, Left to Right)

403 *w/w or Y; Or42b-Gal4, Ubi-FRT-STOP-FRT-mCD8::DQVD::QF2/UASz-*

404 *3xFLAG::mNeonGreen; UAS-FLP, QUAS-tdTomato::3xHA/+*

405 *w/w or Y; Or42b-Gal4, Ubi-FRT-STOP-FRT-mCD8::DQVD::QF2/+; UAS-FLP, QUAS-*
406 *tdTomato::3xHA/UASz-Fas3G::3xFLAG*
407 *w/w or Y; Or42b-Gal4, Ubi-FRT-STOP-FRT-mCD8::DQVD::QF2/UASz-*
408 *Drice::myc::mNeonGreen; UAS-FLP, QUAS-tdTomato::3xHA/+*
409 *w/w or Y; Or42b-Gal4, Ubi-FRT-STOP-FRT-mCD8::DQVD::QF2/UASz-*
410 *Drice::myc::mNeonGreen; UAS-FLP, QUAS-tdTomato::3xHA/UASz-Fas3G::3xFLAG*
411
412 Fig. 4H, I (Top to Bottom, Left to Right)
413 *w/w or Y; Or42b-Gal4, Ubi-FRT-STOP-FRT-mCD8::DQVD::QF2/UASz-*
414 *3xFLAG::mNeonGreen; UAS-FLP, QUAS-tdTomato::3xHA/+*
415 *w/w or Y; Or42b-Gal4, Ubi-FRT-STOP-FRT-mCD8::DQVD::QF2/+; UAS-FLP, QUAS-*
416 *tdTomato::3xHA/UASz-Fas3G::3xFLAG*
417 *w/w or Y; Or42b-Gal4, Ubi-FRT-STOP-FRT-mCD8::DQVD::QF2/UAS-Dronc-RNAi; UAS-*
418 *FLP, QUAS-tdTomato::3xHA/UASz-Fas3G::3xFLAG*
419 *w/w or Y; Or42b-Gal4, Ubi-FRT-STOP-FRT-mCD8::DQVD::QF2/UAS-Dronc^{DN}; UAS-FLP,*
420 *QUAS-tdTomato::3xHA/UASz-Fas3G::3xFLAG*
421
422 Fig. 4K, L (Left to Right)
423 *w/Y; Or42b-Gal4/UASz-3xFLAG::mNeonGreen*
424 *w/Y; Or42b-Gal4/+; +/UASz-Fas3G::3xFLAG*
425 *w/Y; Or42b-Gal4/UAS-Dronc-RNAi; +/UASz-Fas3G::3xFLAG*
426 *w/Y; Or42b-Gal4/UAS-Dronc^{DN}; +UASz-Fas3G::3xFLAG*
427
428 ***Protein preparation from Drosophila tissues***

429 Adult heads or brains of the given genotype were dissected and lysed with RIPA buffer (50 mM
430 Tris-HCl, pH 8.0, 150 mM Sodium Chloride, 0.5 w/v% Sodium Deoxycholate, 0.1% w/v
431 Sodium Dodecyl Sulfate, and 1.0% w/v NP-40) supplemented with cOmplete ULTRA EDTA-
432 free protease inhibitor cocktail (#05892953001, Roche). Samples were homogenized and
433 centrifuged at 20,000 ×g, 4°C for 10 min. The supernatants were collected and snap-frozen in
434 liquid nitrogen. Protein concentrations were determined using the BCA assay (#297-73101,
435 Wako) following the manufacturer's protocol. The samples were mixed with 6x Laemmli
436 buffer, boiled at 95°C for 5 min, and then subjected to purification of biotinylated proteins and
437 western blot analysis.
438
439 ***Western blotting***
440 Each sample was separated using SDS-PAGE. The proteins were then transferred onto
441 Immobilon-P PVDF membranes (#IPVH00010; Millipore) for immunoblotting. Membranes
442 were blocked with 4% skim milk diluted in 1× TBST. Immunoblotting was performed using
443 the antibodies mentioned below diluted in 4% skim milk. Signals were visualized using
444 Immobilon Western Chemiluminescent HRP Substrate (#WBKLS0500; Millipore) and
445 FUSION SOLO. 7S. EDGE imaging station (Vilber-Lourmat). Contrast and brightness
446 adjustments were applied equally using Fiji (ImageJ) software (NIH Image).
447 The primary antibodies used included mouse anti-V5 monoclonal antibody (1:5,000,
448 #46-0705, Invitrogen), mouse anti-FLAG M2 monoclonal antibody (1:5,000, Sigma), mouse
449 anti-alpha tubulin (DM1A) monoclonal antibody (1:10,000, #T9026, Sigma), mouse anti-Actin
450 monoclonal antibody (1:5,000; #A4700, Sigma), mouse anti-Fasciclin 3 (7G10) antibody (1:50,
451 #AB_528238, DSHB), rabbit anti-Fasciclin3 isoform G antibody (1:50, this study). The
452 secondary antibodies used included goat anti-rabbit IgG HRP-conjugated antibody (1:5,000,
453 #7074S, CST) and goat/rabbit/donkey anti-mouse IgG HRP Conjugate (1:5,000, #W402B,

454 Promega). The membranes for streptavidin blotting were blocked with 3% BSA. Streptavidin
455 blotting was performed using streptavidin-horseradish peroxidase (1:10,000, #SA10001;
456 Invitrogen) diluted in 3% BSA.
457
458 ***Immunohistochemistry***
459 Adult brains were dissected in phosphate-buffered saline (PBS) and fixed in 4%
460 paraformaldehyde (PFA) at room temperature for 30 min. Adult brains were washed three times
461 with 0.3% PBST (Triton-X100) for 10 min. After blocking with 5.0% normal donkey serum
462 (#S30, Millipore)/PBST (PBSTn) for 30 minutes at room temperature, tissues were incubated
463 with primary antibody/PBSTn overnight at 4°C. The samples were then washed with PBST
464 three times for 10 min each and incubated with secondary antibody/PBSTn for 2 h at room
465 temperature. After incubation, the tissues were washed with PBST three times for 10 min.
466 Streptavidin and Hoechst 33342 were added during secondary antibody incubation. The
467 samples were mounted on glass slides with SlowFade Gold antifade reagent (#S36939,
468 Invitrogen). Images were captured using a Leica TCS SP8 micrscope (Leica Microsystems).
469 Images were analyzed and edited using the Fiji (ImageJ) software. For MASCaT analysis,
470 newly eclosed adults were raised at 29°C for 1 week. Classification of the MASCaT signal was
471 performed by optically assessing the tdTomato intensity. For cell number analysis, newly
472 eclosed adults were raised at 29°C for 1 week. The antennae were dissected as previously
473 described [36], fixed with 4% PFA at room temperature for 30 min, and washed with 0.4%
474 PBST (Triton-X100) three times for 10 min. Quantification of cell numbers in antenna was
475 performed using Fiji (ImageJ) software using "3D object counter" for RedStinger positive cells.
476 The primary antibodies used were mouse anti-Fasciclin 3 (7G10) antibody (1:20,
477 #AB_528238, DSHB), rat anti-GFP (GF090R) monoclonal antibody (1:100, #04404-26,
478 nacalai Tesque), mouse anti-FLAG M2 monoclonal antibody (1:500, F1804, Sigma), and rat

479 anti-mCD8 monoclonal antibody (1:50, #MCD0800, Invitrogen). The secondary antibodies
480 used included Alexa Fluor 488-conjugated donkey anti-mouse IgG antibody (1:500, #A-21202,
481 ThermoFisher Scientific), Alexa Fluor 488-conjugated donkey anti-rat IgG antibody (1:500,
482 #A-21208, ThermoFisher Scientific), Alexa Fluor 647-conjugated donkey anti-mouse IgG
483 antibody (1:500, #A-31571, ThermoFisher Scientific), and Alexa Fluor 633-conjugated goat
484 anti-rat IgG antibody (1:500, #A-21094, ThermoFisher Scientific). The nuclei were stained
485 with Hoechst 33342 (8 μM, #H3570, Invitrogen). Streptavidin-Cy2 (1:500, #016-220-084,
486 Jackson ImmunoResearch) and Streptavidin-Cy5 (1:500, #016-170-084, Jackson
487 ImmunoResearch) were used to stain the biotinylated proteins.
488
489 ***Experimental design for LC-MS/MS analyses***
490 Two biological replicates were analyzed for each experimental condition to determine the
491 relative abundance of *Drice::V5::TurboID/w*^{1118}.
492
493 ***Purification of biotinylated proteins***
494 Samples were prepared as previously described [17]. Briefly, 100 μg of biotinylated protein-
495 containing lysate was subjected to FG-NeutrAvidin bead (#TAS8848 N1171, Tamagawa Seiki)
496 purification. The FG-NeutrAvidin beads (25 μL, approximately 500 μg) were washed three
497 times with RIPA buffer. Benzonase-treated biotinylated protein samples suspended in 1 mL
498 RIPA buffer were incubated overnight at 4°C. Conjugated beads were magnetically isolated
499 and washed with 500 μL of an ice-cold RIPA buffer solution, 1 M KCl solution, 0.1 M Na_2CO_3
500 solution and 4 M urea solution. For western blot analyses, the purified samples were mixed
501 with Laemmli buffer, boiled at 95°C for 5 min, and then subjected to western blot analysis. For
502 LC-MS/MS analysis, the purified samples were washed with 500 μL ultrapure water (#214-
503 01301, Wako) and 500 μL of 50 mM ammonium bicarbonate (AMBC). The samples were then

504 mixed with 50 μL of 0.1% Rapigest diluted in 50 mM AMBC, and 5 μL of 50 mM TCEP was
505 subsequently added. Samples were incubated at 60°C for 5 min, and then 2.5 μL 200 mM
506 MMTS was added. One microgram sequence-grade modified trypsin (#V5111, Promega) was
507 then added for on-bead trypsin digestion at 37°C for 16 h. The beads were magnetically isolated
508 and 60 μL of the supernatant was collected. Then, 3 μL 10% TFA was added to the
509 supernatants, and the samples were incubated at 37°C for 60 min with gentle agitation. The
510 samples were then centrifuged at 20,000 ×g, 4°C for 10 min. The peptides were desalinated and
511 purified using a GL-tip SDB (#7820-11200, GL Sciences) following the manufacturer's
512 protocol. The samples were speed-backed at 45°C for 30 min and dissolved in 25 μL of 0.1%
513 formic acid. The samples were then centrifuged at 20,000 ×g, 4°C for 10 min, and the
514 supernatants were collected. The peptide concentrations were determined using the BCA assay.
515 Finally, 500 ng of the purified protein was subjected to LC-MS/MS analysis.
516
517 ***LC-MS/MS analyses***
518 LC-MS/MS analyses were performed as previously described [17]. Briefly, samples were
519 loaded onto Acclaim PepMap 100 C18 column (75 μm x 2 cm, 3 μm particle size and 100 Å
520 pore size; #164946, ThermoFisher Scientific) and separated on nano-capillary C18 column, (75
521 μm x 12.5 cm, 3 μm particle size, #NTCC-360/75-3-125, Nikkyo Technos) using EASY-nLC
522 1200 system (ThermoFisher Scientific). The elution conditions are listed in Table S3. The
523 separated peptides were analyzed using QExactive (ThermoFisher Scientific) in data-dependent
524 MS/MS mode. The parameters for the MS/MS analysis are listed in Table S4. The collected
525 data were analyzed using Proteome Discoverer (PD) 2.2 software with the Sequest HT search
526 engine. The parameters for the PD 2.2 analysis are described in Table S5. Peptides were filtered
527 at a false discovery rate of 0.01 using the Percolator node. Label-free quantification was
528 performed based on the intensities of the precursor ions using a precursor-ion quantifier node.

529 Normalization was performed using the total amount of peptides in all average scaling modes.
530 Proteins with 10 folds or higher abundance relative to the control (w^{1118}) were considered for
531 further analysis. MS proteomic data were deposited in the ProteomeXchange Consortium via
532 the jPOST partner repository with the dataset identifier PXD042922 [37].
533
534 ***Gene Ontology analysis***
535 Gene Ontology (GO) analysis of cellular components was performed using DAVID [38].
536
537 ***Generation of rabbit polyclonal anti-Fasciclin 3 isoform G antibody***
538 The peptide corresponding to the 506–524 AA (N-LKPANEATPATTPAPTTAA-C) of Fas3G
539 was used by Eurofins Inc. to immunize rabbits to raise a polyclonal antibody. The antibody was
540 affinity purified using the same peptide provided by Eurofins, Inc.
541
542 ***IDR prediction***
543 Amino acid sequences were obtained from the FlyBase database [https://flybase.org/].
544 Disordered intracellular regions of Fas3 isoforms were predicted using the PSIPRED protein
545 sequence analysis workbench in DISOPRED3 [http://bioinf.cs.ucl.ac.uk/psipred/].
546
547 ***Molecular cloning***
548 For all isoforms (A, B/F, C, D/E, G) of *pUASz-Fasciclin 3::3xFLAG*, the coding sequences of
549 Fasciclin 3s were PCR-amplified using 3xFLAG-tag harboring primers from *Drosophila* cDNA
550 and were ligated into the *BamH*I/*Kpn*I-digested *pUASz1.0* vector [39] using In-Fusion
551 (#Z9648N TaKaRa). For *pUASz-3xFLAG::mNeonGreen*, the coding sequence of mNeonGreen
552 was PCR-amplified using 3xFLAG-tag harboring primers from *pAc5-V5::mNeonGreen* [17]
553 and ligated into the *Xho*I-digested *pUASz1.0* vector [39] using In-Fusion. For *pUASz-*

554 *Drice::myc::mNeonGreen*, the coding sequence of mNeonGreen was PCR-amplified from
555 *pAc5-V5::mNeonGreen* [17] using myc-tag-harboring primers. The coding sequence of Drice
556 was PCR-amplified from *Drosophila* cDNA. The two fragments were then ligated into the
557 *Xho*I-digested *pUASz1.0* vector using In-Fusion. For *pUASz-V5::TurboID* and *pUASz-*
558 *Caspase::V5::TurboID*, the coding sequences of *Dcp-1*, *Drice* and *Dronc* were PCR amplified
559 from *Drosophila* cDNA. The coding sequence of V5::TurboID was PCR-amplified from *V5-*
560 *TurboID-NES_pcDNA3* (#107169; Addgene). The two fragments were then ligated into the
561 *Xho*I-digested *pUASz1.0* vector using In-Fusion. Catalytic dead mutations (Dcp-1: C196G
562 (TGC to GGC), Drice: C211G (TGC to GGC), and Dronc: C318G (TGC to GGC)) were
563 introduced by PCR-based site-directed mutagenesis, and the corresponding fragments were
564 ligated into the *Xho*I-digested *pUASz1.0* vector using In-Fusion. *For pUbi-FRT-STOP-FRT-*
565 *mCD8::DQVD/A::QF2*, the FRT-STOP-FRT cassette sequence was PCR amplified from
566 *pJFRC201-10xUAS-FRT-STOP-FRT-myr::smGFP-HA* (#63166; Addgene). The coding
567 sequence of mCD8::DQVD/A was PCR-amplified from the genomic DNA of *Caspase-*
568 *Sensitive/Insensitive-Gal4* [20]. The coding sequence of QF2 was PCR amplified from the
569 *pBPQUw* plasmid [40]. The three fragments were ligated into *EcoR*I-digested *pUbi83* vector (a
570 gift from D. Umetsu) using In-Fusion. For *pQUAST-mNeonGreen*, the coding sequence of
571 mNeonGreen was PCR-amplified from *pAc5-V5::mNeonGreen* [17] and ligated into the *EcoR*I-
572 digested *pQUAST* (#24349, Addgene) vector using In-Fusion. For *pUASz-FLPo*, the coding
573 sequences of FLPo were PCR-amplified from *pQUAST-FLPo* (#24357, Addgene) and ligated
574 into the *Xho*I-digested *pUASz1.0* vector [39] using In-Fusion.

575 All established plasmids were sequenced by Eurofins, Inc. The detailed plasmid DNA
576 sequences are available upon request. The established plasmids were injected into y^1, w^{67c23};
577 *P[CaryP]attP40* (*pUASz-3xFLAG::mNeonGreen* and *pUASz-Drice::myc::mNeonGreen*) or y^1,
578 w^{67c23}; *P[CaryP]attP2* (*pUASz-Fasciclin 3::3xFLAGs* and *pUbi-FRT-STOP-FRT-*

579 *mCD8::DQVD/A::QF2*) for PhiC31-mediated transgenesis (BestGene Inc.). Each red-eye-
580 positive transformant was isogenized. Integration of the attP landing site was confirmed using
581 genomic PCR.
582
583 ***Cell culture***
584 *Drosophila* S2 cells were grown at 25°C in Schneider's *Drosophila* medium (#21720001,
585 GIBCO) supplemented with 10% (v/v) heat-inactivated fetal bovine serum, 100 U/ml penicillin,
586 and 100 μg/ml streptomycin (#168-23191, WAKO). Cells were seeded in 24-well plates and
587 transfected with the desired plasmids using Effectene Transfection Reagent (#301427,
588 QIAGEN) following the manufacturer's protocol. Sixteen hours after transfection, the cells
589 were reseeded into CELL CULTURE DISH, PS, 35/10 MM (#627870, Grainer BIO-ONE) and
590 incubated for 24 h. Images were obtained using a Leica AF6000 DMI6000 B microscope (Leica
591 Microsystems). Images were analyzed and edited using Fiji software (NIH Image).
592
593 ***Aging experiment***
594 Adult male flies were raised in vials containing 15 fly/vial, and incubated at 29℃, 65%
595 humidity with 12h/12h light/dark cycle. The flies were transferred every 2–4 days to vials
596 containing fresh food.
597
598 ***Two choice preference assay***
599 Newly eclosed adult male flies were raised in vials containing 25 fly/vial, and incubated at 29℃,
600 65% humidity with 12h/12h light/dark cycle. The flies were transferred every 2–4 days to vials
601 containing fresh food for 1 week. The flies were starved in MilliQ (MQ) for 4 h prior to the
602 assay. About 75 flies were put in 1000-mL glass beaker, which contained two standards bottles
603 filled with 500 μl 1% ACV and 500 μl MQ. The bottles were then covered with sponge plugs

604 containing pipette tips. The pipette tip was cut to increase the size of the opening such that only
605 one fly could climb into the bottle at a time. The glass beaker was covered with a mesh fabric.
606 The beakers were set in an incubator at 29°C for 2 hr for the assay. The experiments were
607 evaluated only if at least one of the tested flies entered either of 2 bottles. The preference index
608 equaled the number of flies in the ACV minus the number of flies in the MQ, divided by the
609 number of flies in both bottles and fields, and multiplied by 100. Values greater than zero
610 indicate a preference for 1% ACV and values less than zero indicate aversion. We repeated the
611 same experiment with different sets of flies and the number of times is indicated by N.
612
613 ***Statistical analysis***
614 Statistical analyses were performed using the GraphPad Prism 8 software (MDF). Data are
615 shown as the means ± standard error of the mean. *P*-values were calculated using a one-way
616 analysis of variance (ANOVA) with Bonferroni correction (Fig. 4B for selected pairs, Fig. 4D
617 for every pair). *P*-values were calculated using the chi-square test with Bonferroni's correction,
618 with mNeonGreen as a control (Fig. 4G), mNeonGreen and Fas3G as controls (Fig. 4I), and
619 mNeonGreen as a control (Fig. 4L). *P*-values were calculated using one-way ANOVA with
620 Dunnett's multiple comparison test (Fig. 4K, mNeonGreen as a control). NS: $P > 0.05$, †: <
621 0.05.

Acknowledgments

We would like to thank Dr. D. Umetsu for providing plasmids, Dr. Y. Nitta, Dr. A. Sugie, and Dr. T. Ichinose for helpful discussions, and the Bloomington *Drosophila* Stock Center and Vienna Drosophila Resource Center for providing the fly strains. We thank Dr. S. Hirayama, Dr. S. Murata, and the one-stop sharing faculty center for future drug discovery at the Graduate School of Pharmaceutical Sciences, University of Tokyo, for the LC-MS/MS analysis. We thank Miura's lab members for their technical assistance and discussions; in particular, K. Takenaga for preparing the fly food, and R. Takamoto for experimental support. The MASCaT was established by MASaya Muramoto with critical advice from members of Shu MASuda at MASayuki Miura Laboratories. We would like to thank *Editage* (www.editage.com) for English language editing of this manuscript.

633 **References**

634 1. Green DR. The Coming Decade of Cell Death Research: Five Riddles. Cell. 2019;177:
635 1094–1107. doi:10.1016/j.cell.2019.04.024
636 2. Nakajima YI, Kuranaga E. Caspase-dependent non-apoptotic processes in development.
637 Cell Death Differ. 2017;24: 1422–1430. doi:10.1038/cdd.2017.36
638 3. Ohsawa S, Hamada S, Kuida K, Yoshida H, Igaki T, Miura M. Maturation of the
639 olfactory sensory neurons by Apaf-1/caspase-9–mediated caspase activity. Proc Natl
640 Acad Sci U S A. 2010;107: 13366–13371. doi:10.1073/pnas.0910488107
641 4. Li Z, Jo J, Jia JM, Lo SC, Whitcomb DJ, Jiao S, et al. Caspase-3 activation via
642 mitochondria is required for long-term depression and AMPA receptor internalization.
643 Cell. 2010;141: 859–871. doi:10.1016/j.cell.2010.03.053
644 5. Aram L, Yacobi-Sharon K, Arama E. CDPs: Caspase-dependent non-lethal cellular
645 processes. Cell Death Differ. 2017;24: 1307–1310. doi:10.1038/cdd.2017.111
646 6. D'Brot A, Chen P, Vaishnav M, Yuan S, Akey CW, Abrams JM. Tango7 directs cellular
647 remodeling by the Drosophila apoptosome. Genes Dev. 2013;27: 1650–1655.
648 doi:10.1101/gad.219287.113
649 7. Kang Y, Neuman SD, Bashirullah A. Tango7 regulates cortical activity of caspases
650 during reaper-triggered changes in tissue elasticity. Nat Commun. 2017;8: 603.
651 doi:10.1038/s41467-017-00693-3
652 8. Orme MH, Liccardi G, Moderau N, Feltham R, Wicky-John S, Tenev T, et al. The
653 unconventional myosin CRINKLED and its mammalian orthologue MYO7A regulate
654 caspases in their signalling roles. Nat Commun. 2016;7: 10972.
655 doi:10.1038/ncomms10972

656 9. Kanuka H, Kuranaga E, Takemoto K, Hiratou T, Okano H, Miura M. Drosophila caspase
657 transduces Shaggy/GSK-3β kinase activity in neural precursor development. EMBO J.
658 2005;24: 3793–3806. doi:10.1038/sj.emboj.7600822
659 10. Amcheslavsky A, Wang S, Fogarty CE, Lindblad JL, Fan Y, Bergmann A. Plasma
660 Membrane Localization of Apoptotic Caspases for Non-apoptotic Functions. Dev Cell.
661 2018;45: 450–464.e3. doi:10.1016/j.devcel.2018.04.020
662 11. Julien O, Wells JA. Caspases and their substrates. Cell Death Differ. 2017;24: 1380–
663 1389. doi:10.1038/cdd.2017.44
664 12. Kumar S. Caspase function in programmed cell death. Cell Death Differ. 2007;14: 32–
665 43. doi:10.1038/sj.cdd.4402060
666 13. Kumar S, Dorstyn L, Lim Y. The role of caspases as executioners of apoptosis. Biochem
667 Soc Trans. 2022;50: 33–45. doi: 10.1042/BST20210751
668 14. Branon TC, Bosch JA, Sanchez AD, Udeshi ND, Svinkina T, Carr SA, et al. Efficient
669 proximity labeling in living cells and organisms with TurboID. Nat Biotechnol. 2018;36:
670 880–887. doi:10.1038/nbt.4201
671 15. Qin W, Cho KF, Cavanagh PE, Ting AY. Deciphering molecular interactions by
672 proximity labeling. Nat Methods. 2021;18: 133–143. doi:10.1038/s41592-020-01010-5
673 16. Shinoda N, Hanawa N, Chihara T, Koto A, Miura M. Dronc-independent basal
674 executioner caspase activity sustains Drosophila imaginal tissue growth. Proc Natl Acad
675 Sci U S A. 2019;116: 20539–20544. doi:10.1073/pnas.1904647116
676 17. Shinoda N, Horikoshi M, Taira Y, Muramoto M, Hirayama S, Murata S, et al. Caspase
677 cleaves Drosophila BubR1 to modulate spindle assembly checkpoint function and
678 lifespan of the organism. FEBS J. 2023; Forthcoming. doi:10.1111/febs.16811
679 18. Chiba A, Snow P, Keshishian H, Hotta Y. Fasciclin III as a synaptic target recognition
680 molecule in Drosophila. Nature. 1995;374: 166–168. doi:10.1038/374166a0

681 19. Kose H, Rose D, Zhu X, Chiba A. Homophilic synaptic target recognition mediated by
682 immunoglobulin-like cell adhesion molecule Fasciclin III. Development. 1997;124:
683 4143–4152. doi: 10.1242/dev.124.20.4143.
684 20. Tang HL, Tang HM, Fung MC, Hardwick JM. In vivo Caspase tracker biosensor system
685 for detecting anastasis and non-apoptotic caspase activity. Sci Rep. 2015;5: 9015.
686 doi:10.1038/srep09015
687 21. Ding AX, Sun G, Argaw YG, Wong JO, Easwaran S, Montell DJ. CasExpress reveals
688 widespread and diverse patterns of cell survival of caspase-3 activation during
689 development in vivo. Elife. 2016;5: e10936. doi:10.7554/eLife.10936
690 22. Chihara T, Kitabayashi A, Morimoto M, Takeuchi K, Masuyama K, Tonoki A, et al.
691 Caspase Inhibition in Select Olfactory Neurons Restores Innate Attraction Behavior in
692 Aged Drosophila. PLoS Genet. 2014;10: e1004437. doi:10.1371/journal.pgen.1004437
693 23. Semmelhack JL, Wang JW. Select Drosophila glomeruli mediate innate olfactory
694 attraction and aversion. Nature. 2009;459: 218–223. doi:10.1038/nature07983
695 24. Walsh JG, Cullen SP, Sheridan C, Lüthi AU, Gerner C, Martin SJ. Executioner caspase-
696 3 and caspase-7 are functionally distinct proteases. Proc Natl Acad Sci U S A. 2008;105:
697 12815–12819. doi:10.1073/pnas.0707715105
698 25. Boucher D, Blais V, Denault JB. Caspase-7 uses an exosite to promote poly(ADP ribose)
699 polymerase 1 proteolysis. Proc Natl Acad Sci U S A. 2012;109: 5669–5674.
700 doi:10.1073/pnas.1200934109
701 26. Desroches A, Denault JB. Caspase-7 uses RNA to enhance proteolysis of poly(ADP-
702 ribose) polymerase 1 and other RNA-binding proteins. Proc Natl Acad Sci U S A.
703 2019;116: 21521–21528. doi:10.1073/pnas.1909283116

704 27. Takemoto K, Nagai T, Miyawaki A, Miura M. Spatio-temporal activation of caspase
705 revealed by indicator that is insensitive to environmental effects. J Cell Biol. 2003;160:
706 235–243. doi:10.1083/jcb.200207111
707 28. Valente P, Lignani G, Medrihan L, Bosco F, Contestabile A, Lippiello P, et al. Cell
708 adhesion molecule L1 contributes to neuronal excitability regulating the function of
709 voltage-gated Na+ channels. J Cell Sci. 2016;129: 1878–1891. doi:10.1242/jcs.182089
710 29. Mukherjee A, Williams DW. More alive than dead: Non-apoptotic roles for caspases in
711 neuronal development, plasticity and disease. Cell Death Differ. 2017;24: 1411–1421.
712 doi:10.1038/cdd.2017.64
713 30. Dehkordi MH, Munn RGK, Fearnhead HO. Non-Canonical Roles of Apoptotic Caspases
714 in the Nervous System. Front Cell Dev Biol. 2022;10: 840023.
715 doi:10.3389/fcell.2022.840023
716 31. Gu Q, Jiao S, Duan K, Wang YX, Petralia RS, Li Z. The BAD-BAX-Caspase-3 Cascade
717 Modulates Synaptic Vesicle Pools via Autophagy. J Neurosci. 2021;41: 1174–1190.
718 doi:10.1523/JNEUROSCI.0969-20.2020
719 32. Cheriyamkunnel SJ, Rose S, Jacob PF, Blackburn LA, Glasgow S, Moorse J, et al. A
720 neuronal mechanism controlling the choice between feeding and sexual behaviors in
721 Drosophila. Curr Biol. 2021;31: 4231-4245.e4. doi:10.1016/j.cub.2021.07.029
722 33. Westphal D, Sytnyk V, Schachner M, Leshchyns'ka I. Clustering of the neural cell
723 adhesion molecule (NCAM) at the neuronal cell surface induces caspase-8- and -3-
724 dependent changes of the spectrin meshwork required for NCAM-mediated neurite
725 outgrowth. J Biol Chem. 2010;285: 42046–42057. doi:10.1074/jbc.M110.177147
726 34. Luck K, Kim DK, Lambourne L, Spirohn K, Begg BE, Bian W, et al. A reference map
727 of the human binary protein interactome. Nature. 2020;580: 402–408.
728 doi:10.1038/s41586-020-2188-x

729 35. Li L, Ding Z, Pang TL, Zhang B, Li CH, Liang AM, et al. Defective minor spliceosomes
730 induce SMA-associated phenotypes through sensitive intron-containing neural genes in
731 Drosophila. Nat Commun. 2020;11: 5608. doi:10.1038/s41467-020-19451-z
732 36. Karim MR, Endo K, Moore AW, Taniguchi H. Whole mount immunolabeling of
733 olfactory receptor neurons in the Drosophila antenna. J Vis Exp. 2014; 51245.
734 doi:10.3791/51245
735 37. Okuda S, Watanabe Y, Moriya Y, Kawano S, Yamamoto T, Matsumoto M, et al.
736 JPOSTrepo: An international standard data repository for proteomes. Nucleic Acids Res.
737 2017;45: D1107–D1111. doi:10.1093/nar/gkw1080
738 38. Huang DW, Sherman BT, Lempicki RA. Bioinformatics enrichment tools: Paths toward
739 the comprehensive functional analysis of large gene lists. Nucleic Acids Res. 2009;37:
740 1–13. doi:10.1093/nar/gkn923
741 39. Deluca SZ, Spradling AC. Efficient expression of genes in the drosophila germline using
742 a uas promoter free of interference by hsp70 pirnas. Genetics. 2018;209: 381–387.
743 doi:10.1534/genetics.118.300874
744 40. Kashio S, Obata F, Zhang L, Katsuyama T, Chihara T, Miura M. Tissue nonautonomous
745 effects of fat body methionine metabolism on imaginal disc repair in Drosophila. Proc
746 Natl Acad Sci U S A. 2016;113: 1835–1840. doi:10.1073/pnas.1523681113
747

748 **Figures & Figure Legends**

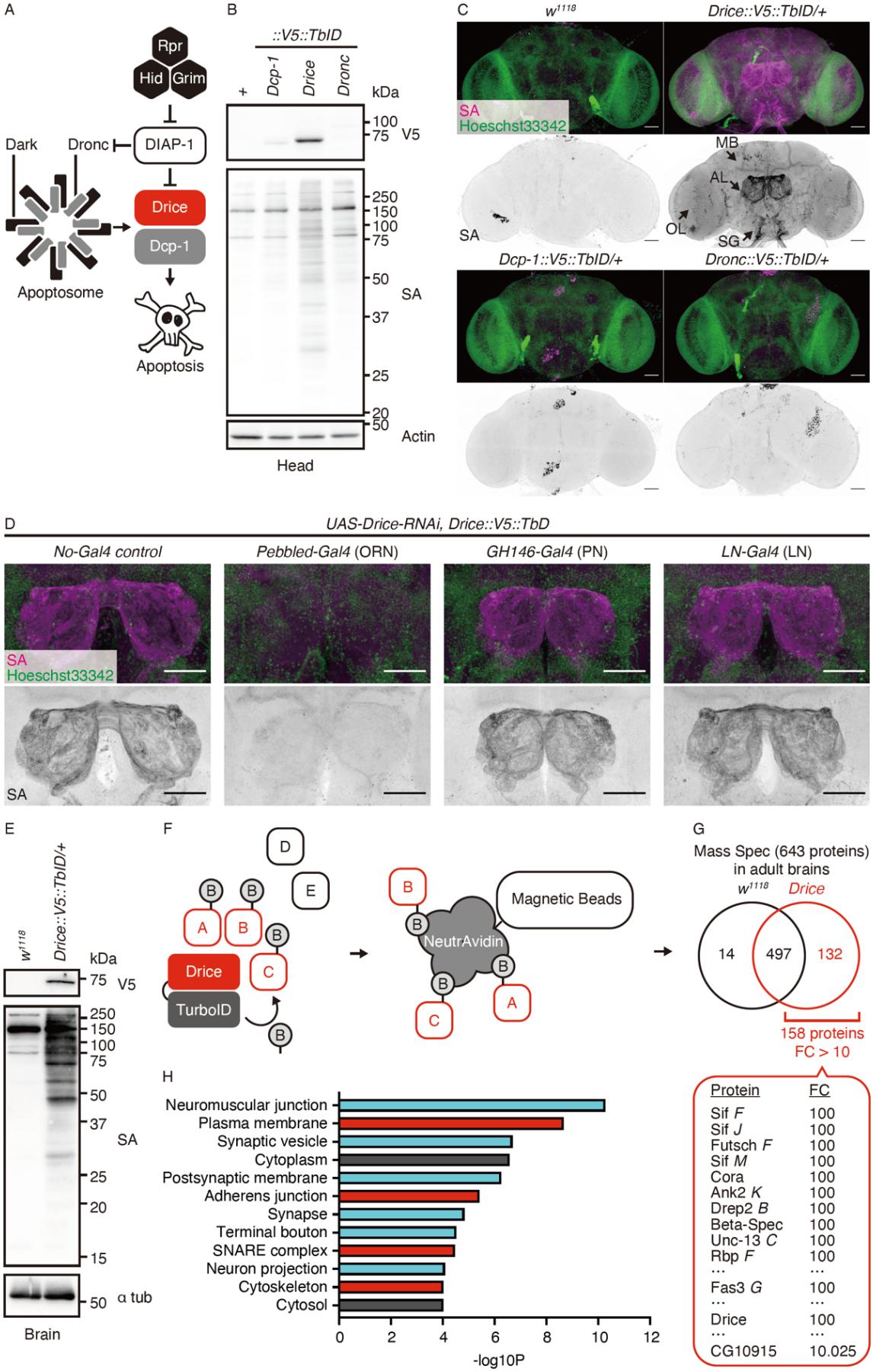

749 **Fig 1. Expression patterns and proximal proteins of Drice in the adult brain.**

750 (A) Schematic diagram of *Drosophila* apoptosis signaling. (B) Western blot of expression of
751 caspases in adult male heads. (C) Representative images of adult male brains. Expression
752 patterns of each caspase are visualized using Streptavidin (SA, magenta). Scale bar: 50 μm. (D)
753 Representative images of antennal lobes (ALs) in the adult female brains. Expression patterns
754 of Drice are visualized using SA (magenta). Scale bar: 50 μm. (E) Western blot of proteins
755 extracted from adult male brains. (F) Schematic diagram of the TurboID-mediated
756 identification of proximal proteins. (G) A summary of mass spectrometry analysis of proteins
757 of the adult male brains. Partial list of Drice proximal proteins and their Fold Change (FC) are
758 shown. (H) Gene Ontology analysis (Cellular Compartment) of 158 Drice proximal proteins
759 (*Drice::V5::TurboID*/w^{1118} > 10). Cyan: neural-related fraction, Red: membrane fraction.

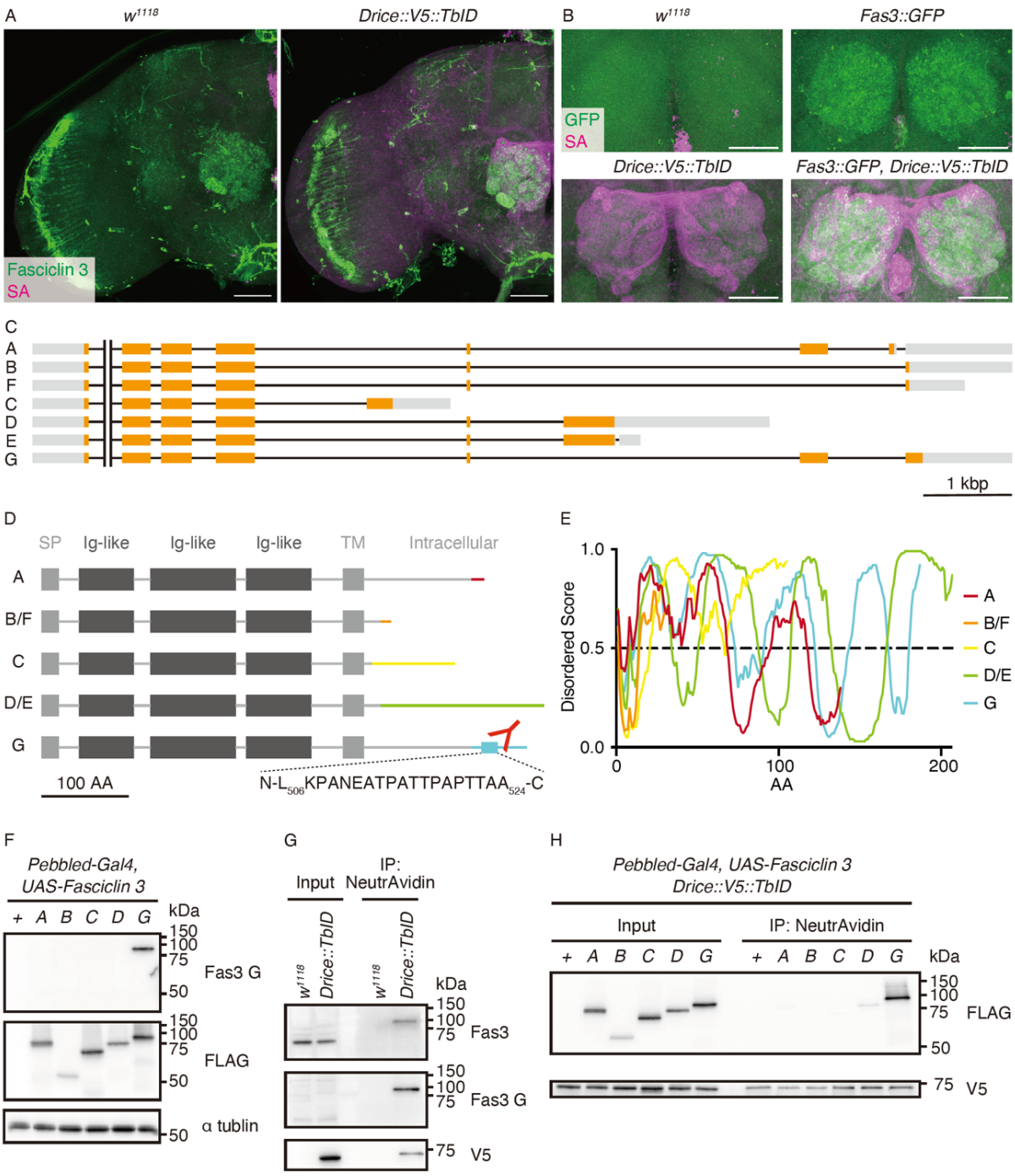

760 **Fig 2. A specific isoform of Fasciclin 3 is in proximity to Drice.**

761 (A) Representative expression patterns of Drice (Streptavidin (SA); magenta) and Fasciclin 3
762 (Fas3, anti-Fasciclin 3 antibody staining; green) in the adult male brains. Scale bar: 50 μm. (B)
763 Representative expression patterns of Drice (SA; magenta) and Fas3 (anti-GFP antibody
764 staining; green) in the antennal lobes (ALs) of the adult male brains. Scale bar: 50 μm. (C) Gene
765 structure of Fas3. CDS (orange) and UTR (grey) are shown in boxes. (D) Schematic structures

766 of Fas3 protein isoforms. Intracellular regions differ from each other. A peptide region used to
767 raise anti-Fas3G antibody is shown. (E) IDR predictions of intracellular regions of each protein
768 isoform. (F) Western blot of proteins extracted from adult heads. Anti-Fas3G antibody
769 specifically detects Fas3 isoform G. (G) Western blot of adult male heads. Drice proximal
770 proteins were purified using NeturAvidin. (H) Western blot of adult head proteins. Drice
771 proximal proteins were purified using NeturAvidin.

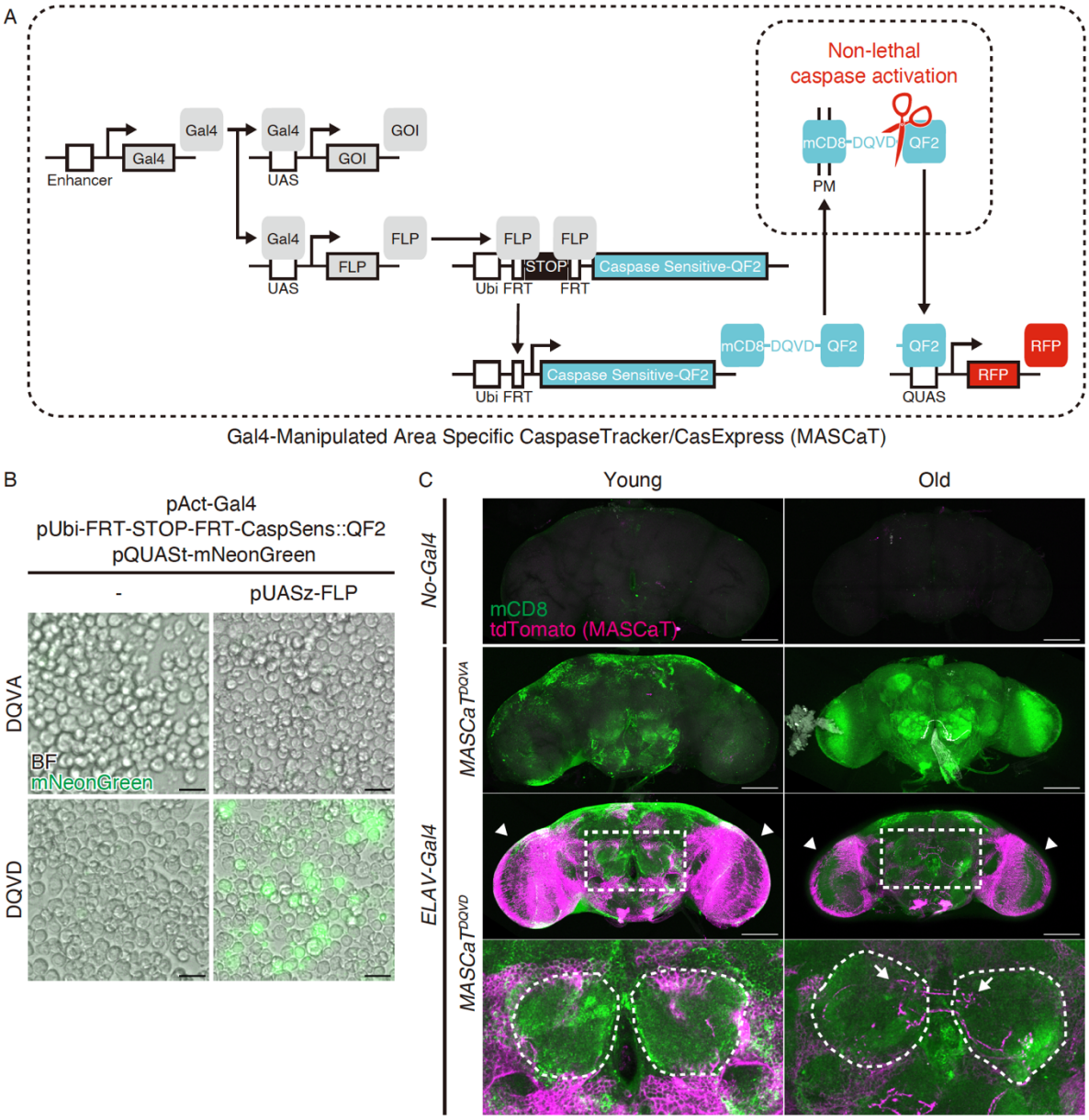

Fig 3. A Gal4-Manipulated Area Specific CaspaseTracker/CasExpress (MASCaT). (A) A schematic diagram of MASCaT expressed using the Gal4/UAS system with FLP-mediated recombination. Caspase sensitive-QF2 is activated by caspase-mediated cleavage at the plasma membrane. (B) Representative images of S2 cells expressing MASCaT. Scale bar: 20 µm. (C) Representative images of adult male brains of young (1 week old) and old (3 weeks old) flies raised at 29°C. Arrowheads indicate optic lobes. Magnified images (white rectangle) show antennal lobes (ALs; white circles). Arrows indicate age-dependent caspase activation at the ALs. Scale bar: 100 µm.

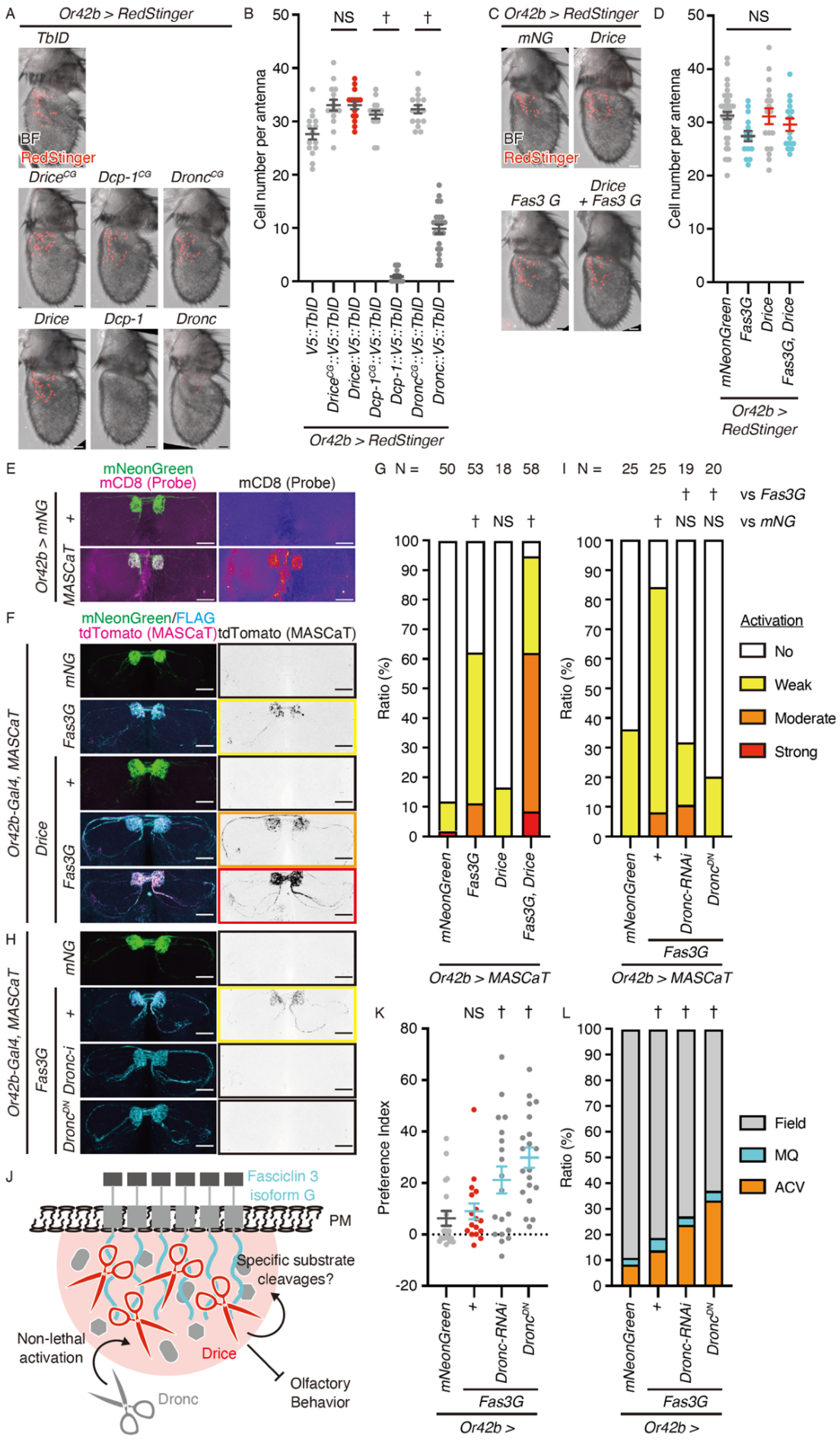
A
Or42b > RedStinger
TbID
BF
RedStinger
Drice^CG
Dcp-1^CG
Dronc^CG
Drice
Dcp-1
Dronc
B
Cell number per antenna
NS
†
†
V5::TbID
Drice^CG::V5::TbID
Drice::V5::TbID
Dcp-1^CG::V5::TbID
Dcp-1::V5::TbID
Dronc^CG::V5::TbID
Dronc::V5::TbID
Or42b > RedStinger
C Or42b > RedStinger
mNG
Drice
BF
RedStinger
Fas3 G
Drice + Fas3 G
D
Cell number per antenna
NS
mNeonGreen
Fas3G
Drice
Fas3G, Drice
Or42b > RedStinger
E
mNeonGreen
mCD8 (Probe)
mCD8 (Probe)
Or42b > mNG
+
MASCaT
F
mNeonGreen/FLAG
tdTomato (MASCaT)
tdTomato (MASCaT)
Or42b-Gal4, MASCaT
mNG
Fas3G
Drice
+
Fas3G
G N = 50 53 18 58
† NS †
Ratio (%)
mNeonGreen
Fas3G
Drice
Fas3G, Drice
Or42b > MASCaT
I N = 25 25 19 20
† †
vs Fas3G
† NS NS
vs mNG
Ratio (%)
mNeonGreen
+
Dronc-RNAi
Dronc^DN
Fas3G
Or42b > MASCaT
Activation
No
Weak
Moderate
Strong
H
Or42b-Gal4, MASCaT
mNG
Fas3G
+
Dronc-i
Dronc^DN
J
Fasciclin 3
isoform G
PM
Specific substrate
cleavages?
Non-lethal
activation
Drice
Dronc
Olfactory
Behavior
K
NS † †
Preference Index
mNeonGreen
+
Dronc-RNAi
Dronc^DN
Fas3G
Or42b >
L
† † †
Ratio (%)
Field
MQ
ACV
mNeonGreen
+
Dronc-RNAi
Dronc^DN
Fas3G
Or42b >

780

781 **Fig 4. Fasciclin 3 isoform G regulates non-lethal caspase activation and functions.**
782 **(**A) Representative images of the adult male antennas of 1 weeks old flies raised at 29°C. Cell
783 bodies are visualized using RedStinger. Scale bar: 20 μm. (B) Quantification of cell number of
784 (A). Data are presented as mean ± SEM. *P*-values were calculated using one-way analysis of
785 variance (ANOVA) with Bonferroni's correction for selected pairs. NS: $P > 0.05$, †: $P < 0.05$.
786 (C) Representative images of the adult male antennas of 1 week old flies raised at 29°C. Cell
787 bodies are visualized using RedStinger. Scale bar: 20 μm. (D) Quantification of cell number of
788 (C). Data are presented as mean ± SEM. *P*-values were calculated using one-way ANOVA with
789 Bonferroni's correction for every pair. NS: $P > 0.05$, †: $P < 0.05$. (E) Representative images of
790 the antennal lobes (ALs) of male brains of 1 week old flies raised at 29°C expressing MASCaT
791 probe (mCD8). Scale bar: 30 μm. (F) Representative images of the ALs of male brains of 1
792 week old flies raised at 29°C with caspase activation visualized by MASCaT. Scale bar: 30 μm.
793 (G) Quantifications of caspase activity detected by MASCaT of (F). *P*-values were calculated
794 using chi-square test with Bonferroni's correction using mNeonGreen as control. NS: $P > 0.05$,
795 †: $P < 0.05$. Sample sizes are shown in the graph. (H) Representative images of the AL of male
796 brains of 1 week old flies raised at 29°C with caspase activation visualized using MASCaT.
797 Scale bar: 30 μm. (I) Quantifications of caspase activity detected using MASCaT of (H). *P*-
798 values were calculated using chi-square test with Bonferroni's correction using mNeonGreen
799 and Fas3G as control, respectively. NS: $P > 0.05$, †: $P < 0.05$. Sample sizes are shown in the
800 graph. (J) A schematic model of compartmentalized non-lethal caspase activation mediated by
801 Fas3G and Dronc. (K) Preference index of 1 week old male flies raised at 29°C in response to
802 1% apple cider vinegar in two choice preference assay. Data are presented as mean ± SEM. *P*-
803 values were calculated using one-way ANOVA followed by Dunnets' multiple comparison test
804 using mNeonGreen as a control. NS: $P > 0.05$, †: $P < 0.05$. Sample sizes: mNG (N = 19 (1327
805 flies)), Fas3G (N = 17 (1191 flies)), Fas3G + Dronc-RNAi (N = 19 (1295 flies)), Fas3G +

806 $Dronc^{DN}$ (N = 20 (1320 flies)). (L) The ratio of flies in the given conditions in the two choice
807 preference assay of (K). *P*-values were calculated using chi-square test with Bonferroni's
808 correction using mNeonGreen as control. †: $P < 0.05$. Sample sizes: mNG (N = 1327 flies),
809 Fas3G (N = 1191 flies), Fas3G + Dronc-RNAi (N = 1295 flies), Fas3G + $Dronc^{DN}$ (N = 1320
810 flies).

811 **Legends for Table S1–5**

812 **Table S1. Proximal protein list.** A list of the identified proximal proteins (Abundance ratio
813 (Drice-V5-TurboID/Control) > 10). The UniProt Accessions, Gene Description, and
814 Abundance Ratio (Drice-V5-TurboID/Control) are listed.

815

816 **Table S2. Gene Ontology analysis.** The result of Gene Ontology (GO) analysis of Cellular
817 Compartment for Drice proximal proteins. GO term, P values, Fold Enrichment, Count and
818 Genes are listed.

819

820 **Table S3. LC settings.** Gradient settings for LC analysis are presented.

821

822 **Table S4. MS/MS settings.** Settings used for the MS/MS analysis are presented.

823

824 **Table S5. Proteome Discoverer 2.2 settings.** Proteome Discoverer 2.2 settings for proteomics
825 analysis are presented.